First observation of the directed flow of D^0 and $\overline{D^0}$ in Au+Au collisions at $\sqrt{s_{\rm NN}}$ = 200 GeV

J. Adam,[12] L. Adamczyk,[2] J. R. Adams,[35] J. K. Adkins,[26] G. Agakishiev,[24] M. M. Aggarwal,[37] Z. Ahammed,[57] I. Alekseev,[3,31] D. M. Anderson,[51] R. Aoyama,[54] A. Aparin,[24] D. Arkhipkin,[5] E. C. Aschenauer,[5] M. U. Ashraf,[53] F. Atetalla,[25] A. Attri,[37] G. S. Averichev,[24] V. Bairathi,[32] K. Barish,[9] A. J. Bassill,[9] A. Behera,[49] R. Bellwied,[19] A. Bhasin,[23] A. K. Bhati,[37] J. Bielcik,[13] J. Bielcikova,[34] L. C. Bland,[5] I. G. Bordyuzhin,[3] J. D. Brandenburg,[46,5] A. V. Brandin,[31] J. Bryslawskyj,[9] I. Bunzarov,[24] J. Butterworth,[42] H. Caines,[60] M. Calderón de la Barca Sánchez,[7] D. Cebra,[7] I. Chakaberia,[25,5] P. Chaloupka,[13] B. K. Chan,[8] F-H. Chang,[33] Z. Chang,[5] N. Chankova-Bunzarova,[24] A. Chatterjee,[57] S. Chattopadhyay,[57] J. H. Chen,[17] X. Chen,[45] J. Cheng,[53] M. Cherney,[12] W. Christie,[5] H. J. Crawford,[6] M. Csanád,[15] S. Das,[10] T. G. Dedovich,[24] I. M. Deppner,[18] A. A. Derevschikov,[39] L. Didenko,[5] C. Dilks,[38] X. Dong,[27] J. L. Drachenberg,[1] J. C. Dunlop,[5] T. Edmonds,[40] N. Elsey,[59] J. Engelage,[6] G. Eppley,[42] R. Esha,[8] S. Esumi,[54] O. Evdokimov,[11] J. Ewigleben,[28] O. Eyser,[5] R. Fatemi,[26] S. Fazio,[5] P. Federic,[34] J. Fedorisin,[24] Y. Feng,[40] P. Filip,[24] E. Finch,[48] Y. Fisyak,[5] L. Fulek,[2] C. A. Gagliardi,[51] T. Galatyuk,[14] F. Geurts,[42] A. Gibson,[56] D. Grosnick,[56] A. Gupta,[23] W. Guryn,[5] A. I. Hamad,[25] A. Hamed,[51] J. W. Harris,[60] L. He,[40] S. Heppelmann,[7] S. Heppelmann,[38] N. Herrmann,[18] L. Holub,[13] Y. Hong,[27] S. Horvat,[60] B. Huang,[11] H. Z. Huang,[8] S. L. Huang,[49] T. Huang,[33] X. Huang,[53] T. J. Humanic,[35] P. Huo,[49] G. Igo,[8] W. W. Jacobs,[21] A. Jentsch,[52] J. Jia,[5,49] K. Jiang,[45] S. Jowzaee,[59] X. Ju,[45] E. G. Judd,[6] S. Kabana,[25] S. Kagamaster,[28] D. Kalinkin,[21] K. Kang,[53] D. Kapukchyan,[9] K. Kauder,[5] H. W. Ke,[5] D. Keane,[25] A. Kechechyan,[24] M. Kelsey,[27] Y. V. Khyzhniak,[31] D. P. Kikoła,[58] C. Kim,[9] T. A. Kinghorn,[7] I. Kisel,[16] A. Kisiel,[58] M. Kocan,[13] L. Kochenda,[31] L. K. Kosarzewski,[13] L. Kramarik,[13] P. Kravtsov,[31] K. Krueger,[4] N. Kulathunga Mudiyanselage,[19] L. Kumar,[37] R. Kunnawalkam Elayavalli,[59] J. H. Kwasizur,[21] R. Lacey,[49] J. M. Landgraf,[5] J. Lauret,[5] A. Lebedev,[5] R. Lednicky,[24] J. H. Lee,[5] C. Li,[45] W. Li,[47] W. Li,[42] X. Li,[45] Y. Li,[53] Y. Liang,[25] R. Licenik,[13] T. Lin,[51] A. Lipiec,[58] M. A. Lisa,[35] F. Liu,[10] H. Liu,[21] P. Liu,[49] P. Liu,[47] T. Liu,[60] X. Liu,[35] Y. Liu,[51] Z. Liu,[45] T. Ljubicic,[5] W. J. Llope,[59] M. Lomnitz,[27] R. S. Longacre,[5] S. Luo,[11] X. Luo,[10] G. L. Ma,[47] L. Ma,[17] R. Ma,[5] Y. G. Ma,[47] N. Magdy,[11] R. Majka,[60] D. Mallick,[32] S. Margetis,[25] C. Markert,[52] H. S. Matis,[27] O. Matonoha,[13] J. A. Mazer,[43] K. Meehan,[7] J. C. Mei,[46] N. G. Minaev,[39] S. Mioduszewski,[51] D. Mishra,[32] B. Mohanty,[32] M. M. Mondal,[22] I. Mooney,[59] Z. Moravcova,[13] D. A. Morozov,[39] Md. Nasim,[8] K. Nayak,[10] J. M. Nelson,[6] D. B. Nemes,[60] M. Nie,[46] G. Nigmatkulov,[31] T. Niida,[59] L. V. Nogach,[39] T. Nonaka,[10] G. Odyniec,[27] A. Ogawa,[5] K. Oh,[41] S. Oh,[60] V. A. Okorokov,[31] B. S. Page,[5] R. Pak,[5] Y. Panebratsev,[24] B. Pawlik,[36] D. Pawlowska,[58] H. Pei,[10] C. Perkins,[6] R. L. Pintér,[15] J. Pluta,[58] J. Porter,[27] M. Posik,[50] N. K. Pruthi,[37] M. Przybycien,[2] J. Putschke,[59] A. Quintero,[50] S. K. Radhakrishnan,[27] S. Ramachandran,[26] R. L. Ray,[52] R. Reed,[28] H. G. Ritter,[27] J. B. Roberts,[42] O. V. Rogachevskiy,[24] J. L. Romero,[7] L. Ruan,[5] J. Rusnak,[34] O. Rusnakova,[13] N. R. Sahoo,[51] P. K. Sahu,[22] S. Salur,[43] J. Sandweiss,[60] J. Schambach,[52] W. B. Schmidke,[5] N. Schmitz,[29] B. R. Schweid,[49] F. Seck,[14] J. Seger,[12] M. Sergeeva,[8] R. Seto,[9] P. Seyboth,[29] N. Shah,[47] E. Shahaliev,[24] P. V. Shanmuganathan,[28] M. Shao,[45] F. Shen,[46] W. Q. Shen,[47] S. S. Shi,[10] Q. Y. Shou,[47] E. P. Sichtermann,[27] S. Siejka,[58] R. Sikora,[2] M. Simko,[34] J. Singh,[37] S. Singha,[25] D. Smirnov,[5] N. Smirnov,[60] W. Solyst,[21] P. Sorensen,[5] H. M. Spinka,[4] B. Srivastava,[40] T. D. S. Stanislaus,[56] M. Stefaniak,[58] D. J. Stewart,[60] M. Strikhanov,[31] B. Stringfellow,[40] A. A. P. Suaide,[44] T. Sugiura,[54] M. Sumbera,[34] B. Summa,[38] X. M. Sun,[10] Y. Sun,[45] Y. Sun,[20] B. Surrow,[50] D. N. Svirida,[3] P. Szymanski,[58] A. H. Tang,[5] Z. Tang,[45] A. Taranenko,[31] T. Tarnowsky,[30] J. H. Thomas,[27] A. R. Timmins,[19] D. Tlusty,[12] T. Todoroki,[5] M. Tokarev,[24] C. A. Tomkiel,[28] S. Trentalange,[8] R. E. Tribble,[51] P. Tribedy,[5] S. K. Tripathy,[22] O. D. Tsai,[8] B. Tu,[10] T. Ullrich,[5] D. G. Underwood,[4] I. Upsal,[46,5] G. Van Buren,[5] J. Vanek,[34] A. N. Vasiliev,[39] I. Vassiliev,[16] F. Videbæk,[5] S. Vokal,[24] S. A. Voloshin,[59] F. Wang,[40] G. Wang,[8] P. Wang,[45] Y. Wang,[10] Y. Wang,[53] J. C. Webb,[5] L. Wen,[8] G. D. Westfall,[30] H. Wieman,[27] S. W. Wissink,[21] R. Witt,[55] Y. Wu,[25] Z. G. Xiao,[53] G. Xie,[11] W. Xie,[40] H. Xu,[20] N. Xu,[27] Q. H. Xu,[46] Y. F. Xu,[47] Z. Xu,[5] C. Yang,[46] Q. Yang,[46] S. Yang,[5] Y. Yang,[33] Z. Ye,[42] Z. Ye,[11] L. Yi,[46] K. Yip,[5] I. -K. Yoo,[41] H. Zbroszczyk,[58] W. Zha,[45] D. Zhang,[10] L. Zhang,[10] S. Zhang,[45] S. Zhang,[47] X. P. Zhang,[53] Y. Zhang,[45] Z. Zhang,[47] J. Zhao,[40] C. Zhong,[47] C. Zhou,[47] X. Zhu,[53] Z. Zhu,[46] M. Zurek,[27] and M. Zyzak[16]

(STAR Collaboration)

[1] *Abilene Christian University, Abilene, Texas 79699*

[2]AGH University of Science and Technology, FPACS, Cracow 30-059, Poland
[3]Alikhanov Institute for Theoretical and Experimental Physics, Moscow 117218, Russia
[4]Argonne National Laboratory, Argonne, Illinois 60439
[5]Brookhaven National Laboratory, Upton, New York 11973
[6]University of California, Berkeley, California 94720
[7]University of California, Davis, California 95616
[8]University of California, Los Angeles, California 90095
[9]University of California, Riverside, California 92521
[10]Central China Normal University, Wuhan, Hubei 430079
[11]University of Illinois at Chicago, Chicago, Illinois 60607
[12]Creighton University, Omaha, Nebraska 68178
[13]Czech Technical University in Prague, FNSPE, Prague 115 19, Czech Republic
[14]Technische Universität Darmstadt, Darmstadt 64289, Germany
[15]Eötvös Loránd University, Budapest, Hungary H-1117
[16]Frankfurt Institute for Advanced Studies FIAS, Frankfurt 60438, Germany
[17]Fudan University, Shanghai, 200433
[18]University of Heidelberg, Heidelberg 69120, Germany
[19]University of Houston, Houston, Texas 77204
[20]Huzhou University, Huzhou, Zhejiang 313000
[21]Indiana University, Bloomington, Indiana 47408
[22]Institute of Physics, Bhubaneswar 751005, India
[23]University of Jammu, Jammu 180001, India
[24]Joint Institute for Nuclear Research, Dubna 141 980, Russia
[25]Kent State University, Kent, Ohio 44242
[26]University of Kentucky, Lexington, Kentucky 40506-0055
[27]Lawrence Berkeley National Laboratory, Berkeley, California 94720
[28]Lehigh University, Bethlehem, Pennsylvania 18015
[29]Max-Planck-Institut für Physik, Munich 80805, Germany
[30]Michigan State University, East Lansing, Michigan 48824
[31]National Research Nuclear University MEPhI, Moscow 115409, Russia
[32]National Institute of Science Education and Research, HBNI, Jatni 752050, India
[33]National Cheng Kung University, Tainan 70101
[34]Nuclear Physics Institute of the CAS, Rez 250 68, Czech Republic
[35]Ohio State University, Columbus, Ohio 43210
[36]Institute of Nuclear Physics PAN, Cracow 31-342, Poland
[37]Panjab University, Chandigarh 160014, India
[38]Pennsylvania State University, University Park, Pennsylvania 16802
[39]NRC "Kurchatov Institute", Institute of High Energy Physics, Protvino 142281, Russia
[40]Purdue University, West Lafayette, Indiana 47907
[41]Pusan National University, Pusan 46241, Korea
[42]Rice University, Houston, Texas 77251
[43]Rutgers University, Piscataway, New Jersey 08854
[44]Universidade de São Paulo, São Paulo, Brazil 05314-970
[45]University of Science and Technology of China, Hefei, Anhui 230026
[46]Shandong University, Qingdao, Shandong 266237
[47]Shanghai Institute of Applied Physics, Chinese Academy of Sciences, Shanghai 201800
[48]Southern Connecticut State University, New Haven, Connecticut 06515
[49]State University of New York, Stony Brook, New York 11794
[50]Temple University, Philadelphia, Pennsylvania 19122
[51]Texas A&M University, College Station, Texas 77843
[52]University of Texas, Austin, Texas 78712
[53]Tsinghua University, Beijing 100084
[54]University of Tsukuba, Tsukuba, Ibaraki 305-8571, Japan
[55]United States Naval Academy, Annapolis, Maryland 21402
[56]Valparaiso University, Valparaiso, Indiana 46383
[57]Variable Energy Cyclotron Centre, Kolkata 700064, India
[58]Warsaw University of Technology, Warsaw 00-661, Poland
[59]Wayne State University, Detroit, Michigan 48201
[60]Yale University, New Haven, Connecticut 06520

We report the first measurement of rapidity-odd directed flow (v_1) for D^0 and $\overline{D^0}$ mesons at mid-rapidity ($|y|<0.8$) in Au+Au collisions at $\sqrt{s_{\rm NN}} = 200$ GeV using the STAR detector at the Relativistic Heavy Ion Collider. In 10–80% Au+Au collisions, the slope of the v_1 rapidity dependence (dv_1/dy), averaged over D^0 and $\overline{D^0}$ mesons, is -0.080 ± 0.017 (stat.) ± 0.016 (syst.) for transverse

momentum $p_{\rm T}$ above 1.5 GeV/c. The absolute value of D^0-meson dv_1/dy is about 25 times larger than that for charged kaons, with 3.4σ significance. These data give a unique insight into the initial tilt of the produced matter, and offer constraints on the geometric and transport parameters of the hot QCD medium created in relativistic heavy-ion collisions.

PACS numbers: 25.75.Ld, 25.75.Dw

An important goal of relativistic heavy-ion collisions is to understand the production and dynamics of strongly interacting matter produced at high energy densities [1–8]. The collective motion of particles emitted in such collisions are of special interest because of their sensitivity to the initial stages of the collision, when production of a deconfined Quark-Gluon Plasma (QGP) phase is expected. The directed flow (v_1) of particles is characterized by the first harmonic Fourier coefficient in the azimuthal distribution relative to the reaction plane [9–11]. A hydrodynamic calculation with a tilted initial QGP source [12] can explain the observed negative v_1 slope or "anti-flow" [13] near midrapidity, for charged hadrons measured at RHIC energies [14–16]. However, additional contributions to the directed flow could result from a dipole-like density asymmetry, nuclear shadowing (the interactions between particles and spectators), or a difference in density gradients in different directions within the transverse plane [17–19]. The study of heavy quarks (c and b) in heavy-ion collisions is especially important due to their early creation. Owing to their large masses, heavy quarks are predominantly produced in initial hard scatterings and their relaxation time in the QGP medium is comparable to the lifetime of the QGP. Consequently, heavy quarks are an excellent probe to study QGP dynamics [20].

The transverse momentum ($p_{\rm T}$) spectra and elliptic flow (v_2) of D^0 mesons at midrapidity have been measured at RHIC [21, 22] and LHC [23–25] energies. The magnitude of v_2 for the charm hadrons is found to follow the number-of-constituent-quark (NCQ) scaling pattern observed for light hadron species in non-central heavy-ion collisions [21, 26–28]. Furthermore, charm hadron yields are observed to be significantly suppressed at high $p_{\rm T}$, similar to light hadron species in central heavy-ion collisions. Simultaneous descriptions of charm v_2 and nuclear modification factors ($R_{\rm AA}$) [22, 29–31] have been used to constrain the QGP transport parameters for heavy quarks, such as its drag and diffusion coefficients.

A recent model calculation utilizing Langevin dynamics coupled to a hydrodynamic medium with a tilted initial source, predicted a significantly larger v_1 for D-mesons compared to light flavor hadrons [32]. A notable feature is the strong sensitivity of D-meson v_1 to the initial tilt of the QGP source compared to that of light hadrons. The magnitude of the observed heavy quark v_1 is also sensitive to the QGP transport parameters in the hydrodynamic calculation.

It is further predicted that the transient magnetic field generated in heavy-ion collisions can induce a larger directed flow for heavy quarks than for light quarks due to the Lorentz force [33, 34]. The v_1 induced by this initial electromagnetic (EM) field is expected to have the same magnitude, but opposite charge sign for charm (c) and anti-charm ($\bar{c}$) quarks. This suggests that the v_1 measurements of heavy quarks could offer crucial insight into the properties of the initial EM field. A hydrodynamic model calculation which includes both the initially tilted source and the EM field predicts that the D-mesons will have a significant v_1 as a function of rapidity (y) and a splitting is to be expected between D-mesons and $\overline{D}$-mesons due to the initial magnetic field [35].

In this Letter, we report the first measurement of rapidity-odd directed flow for D^0 and $\overline{D^0}$ mesons in Au+Au collisions at $\sqrt{s_{\rm NN}} = 200\,{\rm GeV}$ in the STAR experiment [36]. We utilize the Heavy Flavor Tracker (HFT) [37, 38], a high-resolution silicon detector consisting of four cylindrical layers. Beginning at the largest radius, there is one layer of Silicon Strip Detector (SSD), one layer of Intermediate Silicon Tracker (IST), and two layers of Pixel Detectors (PXL). The reconstruction of heavy-flavor hadrons is greatly enhanced due to the excellent track pointing resolution and secondary vertex resolution offered by the HFT. STAR collected minimum-bias (MB) triggered events with the HFT during the years 2014 and 2016. The MB events were selected by a coincidence between the east and west Vertex Position Detectors (VPD) [39] located at pseudorapidity $4.4 < |\eta| < 4.9$. To ensure good HFT acceptance, the reconstructed primary vertex along the z-direction is required to be within 6 cm of the center of the detector. Approximately 2.2 billion MB triggered good quality events are used in this analysis.

The D^0 and $\overline{D^0}$ mesons are reconstructed via their hadronic decay channel: $D^0(\overline{D^0}) \rightarrow K^-\pi^+(K^+\pi^-)$ (branching fraction 3.89%, $c\tau \sim 123$ μm). Hereafter, D^0 refers to the combined D^0 and $\overline{D^0}$ samples, unless explicitly stated otherwise. The charged particle tracks are reconstructed using the Time Projection Chamber (TPC) [40] together with the HFT in a uniform 0.5 T magnetic field. The collision centrality is determined from the number of charged particles within $|\eta| < 0.5$ and corrected for trigger inefficiency using a Monte Carlo Glauber simulation [41]. Good quality tracks are ensured by requiring a minimum of 20 TPC hits (out of a possible 45), hits in both layers of PXL, at least one hit in the IST or SSD layer. Further, the tracks are required to

have transverse momentum $p_{\rm T} > 0.6$ GeV/c and pseudorapidity $|\eta| < 1$. The D^0 decay daughters are identified via specific ionization energy loss (dE/dx) inside the TPC and from $1/\beta$ measurements by the Time of Flight (TOF) [42] detector. To identify particle species, the dE/dx is required to be within three and two standard deviations from the expected values for π and K, respectively. When tracks are associated with the hits in the TOF detector, the $1/\beta$ is required to be within three standard deviations from the expected values for both π and K.

The D^0 decay vertex is reconstructed as the mid-point of the distance of closest approach between the two decay daughter tracks. Background arises due to random combinations of tracks passing close to the collision point. The decay topological cuts are tuned to reduce the background and enhance the signal-to-background ratio. The topological cut variables are optimized using the Toolkit for Multivariate Data Analysis (TMVA) package [43] and are discussed in Refs. [21, 31].

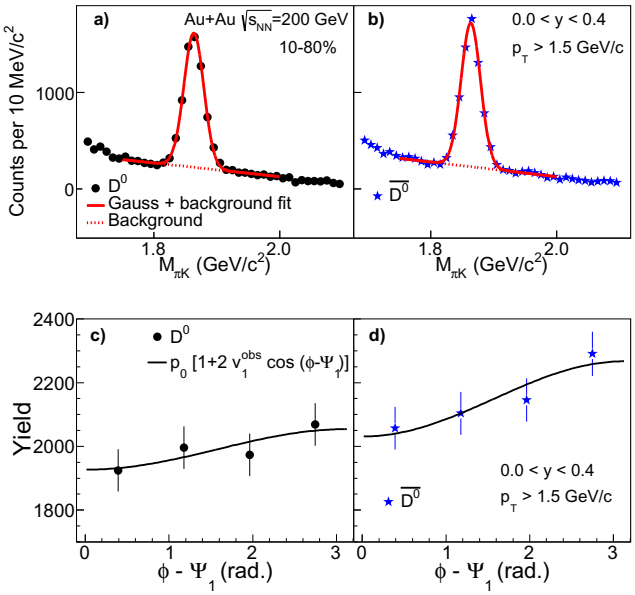

FIG. 1: D^0 (panel (a)) and $\overline{D^0}$ (panel (b)) invariant mass distribution for $0.0 < y < 0.4$ and $p_{\rm T} > 1.5$ GeV/c in 10–80% central Au+Au collisions at $\sqrt{s_{\rm NN}} = 200$ GeV. The solid line represents a Gaussian fit plus a linear function for the random combinatorial background. D^0 (panel (c)) and $\overline{D^0}$ (panel (d)) yields in azimuthal angle bins relative to the first-order event-plane azimuth ($\phi - \Psi_1$) for $0.0 < y < 0.4$ and $p_{\rm T} > 1.5$ GeV/c in 10–80% central Au+Au collisions at $\sqrt{s_{\rm NN}} = 200$ GeV. The solid line presents a fit to the function $p_0[1+2v_1^{\rm obs}\cos(\phi-\Psi_1)]$. Vertical bars show statistical uncertainties.

The first-order event plane (Ψ_1) is measured by using the east and west Zero Degree Calorimeter Shower Maximum Detectors (ZDC-SMD) [14–16, 44, 45], which are located at $|\eta| > 6.3$. Since the v_1 signal is strong at forward rapidity, the ZDC-SMD provides better first-order event plane resolution than detectors closer to midrapidity. Moreover, the five units of η gap between the ZDC-SMDs and the TPC and HFT significantly reduce possible systematic error in v_1 arising from non-flow effects [10, 11]. Such effects could result from resonances, jets, quantum statistics, and final-state interactions like Coulomb effects. Systematic uncertainties arising from event-plane estimation are at the level of less than 2% and are discussed in Ref. [45].

The D^0 v_1 is calculated using the event plane method [9–11]. Figures 1(a) and 1(b) show the D^0 and $\overline{D^0}$ invariant mass spectra for $0.0 < y < 0.4$ and $p_{\rm T} > 1.5$ GeV/c in 10–80% central Au+Au collisions at $\sqrt{s_{\rm NN}} = 200$ GeV. The choice of 10–80% centrality is driven by the fact that the first-order event plane resolution from ZDC-SMD drops considerably in the 0-10% central collisions. The D^0 acceptance, in rapidity and azimuthal angle, under such kinematic selection cuts is uniform across the measured rapidity region. The invariant mass distributions were fitted with a Gaussian plus a first-order linear polynomial function. The linear function provides a good estimate of the random combinatorial background. The yield is obtained by integrating the distribution in the range $1.82-1.91\,{\rm GeV}/c^2$ and subtracting the background beneath the signal. The $D^0(\overline{D^0})$ yield is obtained in each $\phi-\Psi_1$ bin in four rapidity windows. Figures 1(c) and 1(d) present D^0 and $\overline{D^0}$ yields as a function of $\phi-\Psi_1$ for $0.0 < y < 0.4$. The value of v_1 is calculated by fitting the data with a functional form $p_0[1+2v_1^{\rm obs}\cos(\phi-\Psi_1)]$, indicated by the solid lines in the figure. The ZDC-SMD event plane resolution correction factors are obtained in seven centrality bins. For a wide centrality bin (10–80%), it is determined from the D^0-yield-weighted mean of the individual centrality bins' resolutions using a procedure detailed in Ref. [46]. The final v_1 is corrected by scaling $v_1^{\rm obs}$ with the event plane resolution (0.363).

Systematic uncertainties are assessed by comparing the v_1 obtained from various methods. These comparisons include (i) the fit vs. side-band methods for the background estimation and (ii) various invariant mass fitting ranges and residual background functions (first-order vs. second-order polynomials) for signal extractions, (iii) histogram bin counting vs. functional integration for yield extraction, (iv) varying topological cuts so that the efficiency changes by $\pm$ 50% with respect to the nominal value, (v) varying event and track level quality cuts (vi) varying particle identification cuts. The above comparisons are varied independently to form multiple combinations. For the final systematic uncertainty on the $v_1(y)$ and dv_1/dy, the difference between the default settings and alternative measurements from these sources are added in quadrature. Further, the systematic uncertainty in each rapidity bin is symmetrized by considering the maximum uncertainty between D^0 and $\overline{D^0}$.

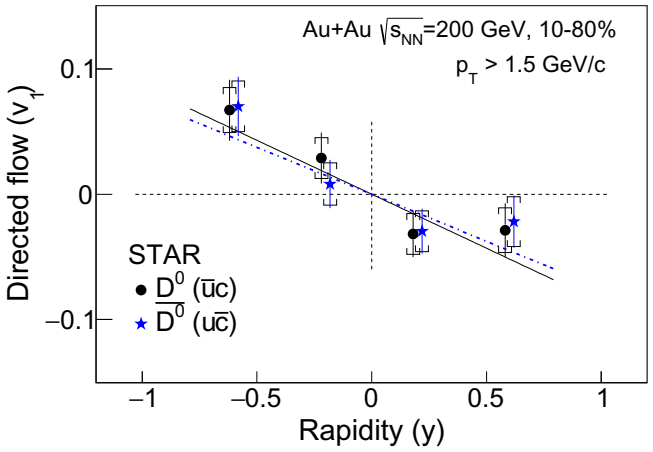

FIG. 2: Filled circles and star symbols present v_1 as a function of rapidity for D^0 and $\overline{D^0}$ mesons at p_T >1.5 GeV/c for 10–80% centrality Au+Au collisions at $\sqrt{s_{NN}}$ = 200 GeV. The D^0 and $\overline{D^0}$ data points are displaced along the x-axis by $\mp$ 0.019 respectively for clear visibility. The error bars and caps denote statistical and systematic uncertainties, respectively. The solid and dot-dashed lines present a linear fit to the data points for D^0 and $\overline{D^0}$, respectively.

In Fig. 2, the filled circle and star markers present the rapidity dependence of v_1 for the D^0 and $\overline{D^0}$ mesons with p_T > 1.5 GeV/c in 10–80% Au+Au collisions at $\sqrt{s_{NN}}$ = 200 GeV. It is a common practice to present the strength of v_1 via its slope at midrapidity. The D^0 ($\overline{D^0}$) v_1-slope (dv_1/dy) is calculated by fitting $v_1(y)$ with a linear function constrained to pass through the origin, as shown by the solid (dot-dashed) line in Fig. 2. The dv_1/dy for D^0 and $\overline{D^0}$ is -0.086 ± 0.025 (stat.) $\pm$ 0.018 (syst.) and -0.075 ± 0.024 (stat.) $\pm$ 0.020 (syst.), respectively. Figure 3(a) presents $v_1(y)$ averaged over D^0 and $\overline{D^0}$ (denoted $\langle v_1 \rangle$) for p_T > 1.5 GeV/c. The dv_1/dy for the averaged D^0 mesons using a linear fit is $-0.080 \pm$ 0.017 (stat.) $\pm$ 0.016 (syst.). The p-value and χ^2/NDF for the linear fit passing through the origin are 0.41 and 2.9/3 respectively. To perform a statistical significance test for a null hypothesis for the v_1 of the averaged D^0 and $\overline{D^0}$, we calculate the χ^2 of the measured $\langle v_1 \rangle$ values set to a constant at zero. The resulting χ^2/NDF and p-value are 14.9/4 and 0.005 respectively, indicating that the data prefer a linear fit with a non-zero slope. The D^0 $v_1(y)$ results are compared to charged kaons, shown by open square markers in Fig. 3(a). The kaon $v_1(y)$ is measured for p_T > 0.2 GeV/c. Note that the $\langle p_T \rangle$ for kaons is 0.63 $\pm$ 0.04 GeV/c while that for D^0 mesons is 2.24 $\pm$ 0.02 GeV/c in our measured p_T acceptance for 10–80% Au+Au collisions at $\sqrt{s_{NN}}$ = 200 GeV. The dv_1/dy of charged kaons, fit using a similar linear function, is -0.0030 ± 0.0001 (stat.) $\pm$ 0.0002 (syst.). The inset in Fig. 3(a) presents the ratio of the v_1 of the D^0 and charged kaons. The absolute value of the D^0-mesons dv_1/dy is observed to be about 25 times larger than that of the kaons with a 3.4σ significance. Moreover, among the measurements by the STAR collaboration of $v_1(y)$ for eleven particle species in Au+Au collisions at 200 GeV [45], the nominal value of the D^0 dv_1/dy is the largest.

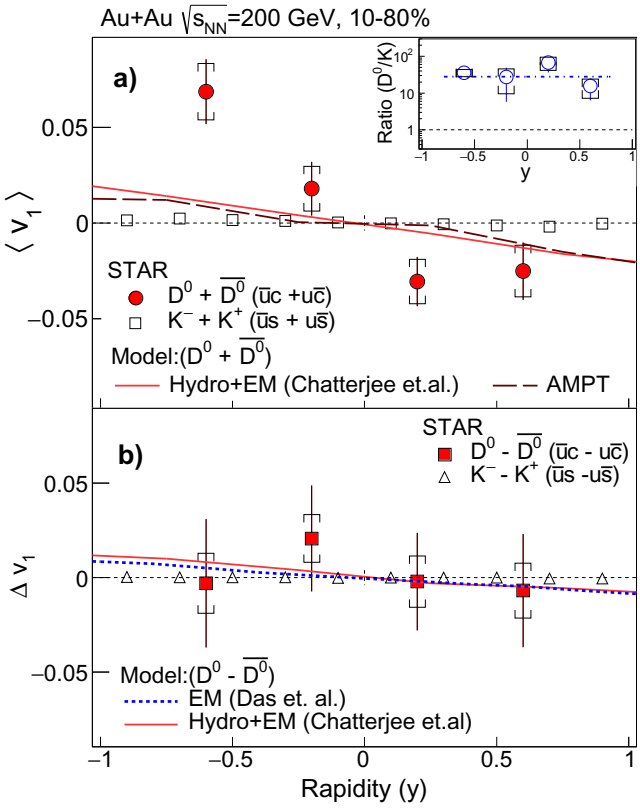

FIG. 3: Panel (a): Solid circles present directed flow ($\langle v_1(y) \rangle$) for the combined samples of D^0 and $\overline{D^0}$ at p_T > 1.5 GeV/c in 10–80% central Au+Au collisions at $\sqrt{s_{NN}}$ = 200 GeV. Open squares present $v_1(y)$ for charged kaons with p_T >0.2 GeV/c. The inset shows the ratio of v_1 between the D^0 and charged kaons. The solid and dashed lines show hydrodynamic model calculation with an initial electromagnetic field [32, 35] and AMPT model [47] calculations, respectively. Panel (b): The solid square markers present the difference in $v_1(y)$ (Δv_1) between D^0 and $\overline{D^0}$ for p_T >1.5 GeV/c in 10–80% Au+Au collisions at $\sqrt{s_{NN}}$ = 200 GeV. Open triangles represent Δv_1 between K^- and K^+. The dotted and solid lines present a Δv_1 prediction for D^0 and $\overline{D^0}$, reported in Refs. [33] and [32, 35], respectively. The error bars and caps denote statistical and systematic uncertainties, respectively.

In hydrodynamic models, the "antiflow" nature of rapidity-odd directed flow is reproduced by an initial tilted source [12], where the tilt parameter is obtained from a fit to $v_1(y)$ for charged hadrons. A recent model calculation [32], where Langevin dynamics for heavy quarks are combined with a hydrodynamic medium and

a tilted initial source, predicted a larger v_1 slope for D mesons compared to light hadrons. It has been argued that the large dv_1/dy for D mesons is driven by the drag from the tilted initial bulk medium. A noteworthy feature in Ref. [32] is the sensitivity of dv_1/dy for D mesons to the tilt parameter. Ref. [32] predicts that the dv_1/dy for D mesons can be 5−20 times larger than for charged hadrons, in qualitative agreement with our data, depending on the choice of tilt and drag parameters.

An initial transient EM field can induce an opposite v_1 for charm and anti-charm quarks. The magnitude of such an induced v_1 is predicted to be several orders of magnitude larger than that for light hadron species due to the early formation of charm quarks [33, 34]. Recently, the authors of Ref. [32] updated their model calculations, and predicted that the D-meson v_1 contribution from the tilted initial source dominates over the contribution from the initial EM-field [35]. The measured D^0 $\langle v_1(y)\rangle$ is compared to such model calculations (solid line) in Fig. 3(a). The model comparison for D^0 plus $\overline{D^0}$ indicates that the model gives the correct sign of dv_1/dy but the v_1 magnitude is underestimated when using the model parameters of Ref. [35]. The current measurements could help to constrain the model parameters such as the tilt and charm drag coefficients.

In Fig. 3(a), the $\langle v_1\rangle$ measurements are also compared to a calculation using A-Multi-Phase-Transport (AMPT) model [47] shown by the dashed line. In this calculation, although the initial rapidity-odd eccentricity (in spatial coordinates) for heavy quarks is smaller than for light quarks, the magnitude of v_1 for heavy flavor hadrons is approximately seven times larger than that for light hadrons at large rapidity. The AMPT calculation also suggests that, as a result of being heavy and produced early, the charm hadrons have an enhanced sensitivity to the initial dynamics, over that for light hadrons. This calculation underpredicts the data.

Figure 3(b) shows the difference between D^0 and $\overline{D^0}$ $v_1(y)$ (denoted Δv_1) measured in 10–80% centrality Au+Au collisions at $\sqrt{s_{\rm NN}} = 200$ GeV. The Δv_1 slope is fitted with a linear function through the origin to give -0.011 ± 0.034 (stat.) $\pm$ 0.020 (syst.). The dashed and solid lines in Fig. 3(b) presents the Δv_1 expectation from two models. The solid line (labeled "Hydro+EM") is the expectation from the model with effects from both a tilted source and an initial EM field [35], while the dotted line is the expectation from the initial EM field only [33]. From these models, the predicted Δv_1 slope for the charm hadrons lie within the range -0.008 to -0.004. However, different values of medium conductivity and time evolution of the EM fields, as well as the description of charm quark dynamics in the QGP can cause large variations in the charge dependent v_1 splitting. The present predictions of Δv_1 are smaller than the current precision of the measurement. Nonetheless, the measurement could provide constraints on the possible variations of the parameters characterizing the EM field and charm quark evolution in the QGP.

In summary, we report the first observation of rapidity-odd directed flow ($v_1(y)$) for D^0 and $\overline{D^0}$ mesons separately, and for their average, in 10–80% central Au+Au collisions at $\sqrt{s_{\rm NN}} = 200$ GeV using the STAR detector at RHIC. The v_1 slope (dv_1/dy) of D^0 mesons are observed to be about a factor of 25 times larger than that for charged kaons with a 3.4σ significance. The observation of a relatively larger and negative v_1 slope for charmed hadrons with respect to the light flavor hadrons can be qualitatively explained by a hydrodynamic model with an initially tilted QGP source [32] and by an AMPT model calculation. These data not only give unique insight into the initial tilt of the produced matter, they are expected to provide improved constraints for the geometric and transport parameters of the hot QCD medium created in relativistic heavy-ion collisions.

We thank the RHIC Operations Group and RCF at BNL, the NERSC Center at LBNL, and the Open Science Grid consortium for providing resources and support. This work was supported in part by the Office of Nuclear Physics within the U.S. DOE Office of Science, the U.S. National Science Foundation, the Ministry of Education and Science of the Russian Federation, National Natural Science Foundation of China, Chinese Academy of Science, the Ministry of Science and Technology of China and the Chinese Ministry of Education, the National Research Foundation of Korea, Czech Science Foundation and Ministry of Education, Youth and Sports of the Czech Republic, Hungarian National Research, Development and Innovation Office (FK-123824), New National Excellency Programme of the Hungarian Ministry of Human Capacities (UNKP-18-4), Department of Atomic Energy and Department of Science and Technology of the Government of India, the National Science Centre of Poland, the Ministry of Science, Education and Sports of the Republic of Croatia, RosAtom of Russia and German Bundesministerium fur Bildung, Wissenschaft, Forschung and Technologie (BMBF) and the Helmholtz Association.

[1] J. C. Collins and M. J. Perry, Phys. Rev. Lett. **34**, 1353 (1975).
[2] S. A. Chin, Phys. Lett. **B78**, 552 (1978).
[3] J. I. Kapusta, Nucl. Phys. **B148**, 461 (1979).
[4] R. Anishetty, P. Koehler, and L. D. McLerran, Phys. Rev. D **22**, 2793 (1980).
[5] I. Arsene *et al.* (BRAHMS), Nucl. Phys. **A757**, 1 (2005).
[6] B. B. Back *et al.* (PHOBOS), Nucl. Phys. **A757**, 28 (2005).
[7] J. Adams *et al.* (STAR), Nucl. Phys. **A757**, 102 (2005).
[8] K. Adcox *et al.* (PHENIX), Nucl. Phys. **A757**, 184 (2005).
[9] J.-Y. Ollitrault, Phys. Rev. D **46**, 229 (1992).

[10] A. M. Poskanzer and S. A. Voloshin, Phys. Rev. C **58**, 1671 (1998).
[11] A. Bilandzic, R. Snellings, and S. Voloshin, Phys. Rev. C **83**, 044913 (2011).
[12] P. Bozek and I. Wyskiel, Phys. Rev. C **81**, 054902 (2010).
[13] J. Brachmann, S. Soff, A. Dumitru, H. Stoecker, J. A. Maruhn, W. Greiner, L. V. Bravina, and D. H. Rischke, Phys. Rev. C **61**, 024909 (2000).
[14] J. Adams *et al.* (STAR), Phys. Rev. C **73**, 034903 (2006).
[15] B. I. Abelev *et al.* (STAR), Phys. Rev. Lett. **101**, 252301 (2008).
[16] L. Adamczyk *et al.* (STAR), Phys. Rev. Lett. **108**, 202301 (2012).
[17] R. J. M. Snellings, H. Sorge, S. A. Voloshin, F. Q. Wang, and N. Xu, Phys. Rev. Lett. **84**, 2803 (2000).
[18] U. W. Heinz and P. F. Kolb, J. Phys. **G30**, S1229 (2004).
[19] L. Adamczyk *et al.* (STAR), Phys. Rev. C **98**, 014915 (2018).
[20] A. Andronic *et al.*, Eur. Phys. J. **C76**, 107 (2016).
[21] L. Adamczyk *et al.* (STAR), Phys. Rev. Lett. **118**, 212301 (2017).
[22] L. Adamczyk *et al.* (STAR), Phys. Rev. Lett. **113**, 142301 (2014), Phys. Rev. Lett. **121**, 229901 (E) (2018).
[23] B. Abelev *et al.* (ALICE), Phys. Rev. Lett. **111**, 102301 (2013).
[24] B. B. Abelev *et al.* (ALICE), Phys. Rev. C **90**, 034904 (2014).
[25] B. Abelev *et al.* (ALICE), JHEP **09**, 112 (2012).
[26] J. Adams *et al.* (STAR), Phys. Rev. Lett. **92**, 052302 (2004).
[27] B. I. Abelev *et al.* (STAR), Phys. Rev. C **75**, 054906 (2007).
[28] S. S. Adler *et al.* (PHENIX), Phys. Rev. Lett. **91**, 182301 (2003).
[29] J. Adams *et al.* (STAR), Phys. Rev. Lett. **91**, 172302 (2003).
[30] S. S. Adler *et al.* (PHENIX), Phys. Rev. C **69**, 034910 (2004).
[31] J. Adam *et al.* (STAR), Phys. Rev. C **99**, 034908 (2019).
[32] S. Chatterjee and P. Bozek, Phys. Rev. Lett. **120**, 192301 (2018).
[33] S. K. Das, S. Plumari, S. Chatterjee, J. Alam, F. Scardina, and V. Greco, Phys. Lett. **B768**, 260 (2017).
[34] U. Gursoy, D. Kharzeev, and K. Rajagopal, Phys. Rev. C **89**, 054905 (2014).
[35] S. Chatterjee and P. Bozek (2018), arXiv:1804.04893.
[36] K. H. Ackermann *et al.* (STAR), Nucl. Instrum. Meth. **A499**, 624 (2003).
[37] D. Beavis *et al.* (STAR Note SN0600) (2011).
[38] G. Contin *et al.*, Nucl. Instrum. Meth. **A907**, 60 (2018).
[39] W. J. Llope *et al.*, Nucl. Instrum. Meth. **A522**, 252 (2004).
[40] M. Anderson *et al.*, Nucl. Instrum. Meth. **A499**, 659 (2003).
[41] B. I. Abelev *et al.* (STAR), Phys. Rev. C **79**, 034909 (2009).
[42] B. Bonner, H. Chen, G. Eppley, F. Geurts, J. Lamas Valverde, C. Li, W. J. Llope, T. Nussbaum, E. Platner, and J. Roberts, Nucl. Instrum. Meth. **A508**, 181 (2003).
[43] H. Voss, A. Hocker, J. Stelzer, and F. Tegenfeldt, PoS **ACAT**, 040 (2007).
[44] G. Wang (PhD thesis, Kent State University) (2005).
[45] L. Adamczyk *et al.* (STAR), Phys. Rev. Lett. **112**, 162301 (2014).
[46] H. Masui, A. Schmah, and A. M. Poskanzer, Nucl. Instrum. Meth. **A833**, 181 (2016).
[47] M. Nasim and S. Singha, Phys. Rev. C **97**, 064917 (2018).